Inorganic Chemistry

ARTICLE

pubs.acs.org/IC

Chlorination and Solvothermal Treatment of $Zr(C_5H_5)_2Cl_2$: a Synthetic Combination to Produce Nanometric Tetragonal ZrO_2

D. Ávila-Brande,*[,†] R. Perezzan,[‡] E. Urones-Garrote,[§] and L. C. Otero-Díaz[†]

[†]Departamento de Química Inorgánica I, [‡]Departamento de Química Física I, Fac. CC. Químicas, and [§]Centro Nacional de Microscopía Electrónica, Universidad Complutense, 28040 Madrid, Spain

ABSTRACT: A novel synthetic strategy based on the combination of the chlorination of an organometallic precursor followed by solvothermal treatment is found to be successful in the synthesis of tetragonal nano-ZrO_2 or nano-ZrO_2, embedded in an amorphous carbon matrix, depending on the solvent employed in the solvothermal step. The chemical and structural features (chemical composition, size and surface defects) of the intermediate and final materials have been determined experimentally mainly by high resolution transmission electron microscopy, electron energy loss spectroscopy, and Z-contrast images. These local techniques reveal that the nanoparticles consist of tetragonal ZrO_2 with an average size of 1.7 ± 0.4 and 6.2 ± 0.9 nm for the embedded in carbon and the free nano-ZrO_2, respectively.

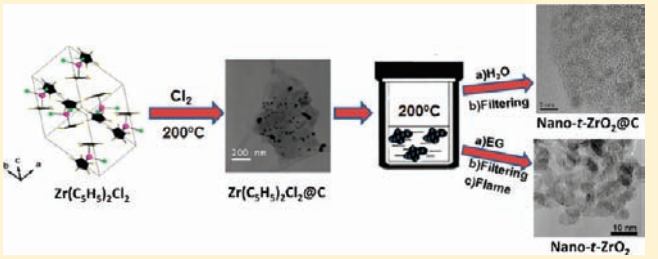

1. INTRODUCTION

Recently, intensive research is focused on the development of nano-oxides, not only for their fundamental scientific interest but also for a variety of technological applications. Novel properties, stabilization of high temperature phases, and high performances are obtained because of not only their small size but also their uniform size distribution. Hence, the development of synthetic methodologies to produce nanoparticles has become one of the most important sections of nanoscience and nanotechnology.[1]

ZrO_2 is one of the most important and investigated ceramic materials because of its number of applications depending on the crystalline phase. The stable phase at room temperature is monoclinic and is important in catalysis,[2] gate dielectrics,[3] and bioactive coatings in bone implants;[4] however, the high temperature phases, tetragonal and cubic, are promising candidates for oxygen sensors,[5] fuel cell electrolytes,[6] and structural materials.[7]

The research in the synthesis of nanoparticles has provided the stabilization of the high-temperature tetragonal phase at room temperature as a consequence of the dominance of the surface energy contribution to the Gibbs free energy of formation in this size range.[8] Examples of these methods include sol−gel,[9] solvothermal,[10] thermal decomposition,[11] emulsion precipitation,[12] and microwave/sonication-assisted coprecipitation[13] approaches.

One of the most successful synthetic methods to produce nanometric ZrO_2 is the solvothermal treatment of molecular zirconium derivatives, such as zirconium(IV) isopropoxide isopropanol complex $(Zr[OCH(CH_3)_2]_4.(CH_3)_2CHOH$ or the mixture of $Zr[OCH(CH_3)_2]_4\cdot(CH_3)_2CHOH$ and $ZrCl_4$, yielding monodisperse nanoparticles.[14] It has also been reported that the solvothermal reaction of zirconium alkoxides in benzyl alcohols leads to 3 nm zirconia particles[15] as well as their homogeneous doping using transition metal ions such as Mn or Cr.[16,17]

The synthesis of nanocomposites is also a focus of research, and methods like magnetron sputtering[18] or pulsed direct current plasma-enhanced chemical vapor deposition[19] have been successfully applied in the growth of films of ZrO_2-carbon. In these thin films some properties such as hardness can be improved,[18] or some other undesirable such as the aging of implants based in pure ZrO_2 can be reduced.[19]

However, a synthetic strategy to produce either nanometric ZrO_2 or nano-ZrO_2 embedded in an amorphous carbonaceous matrix, using a single Zr metal−organic derivative as precursor has not been reported yet.

Among the multiple methods to produce nanostructured carbons, a well-established one consists of the selective etching of the metal atoms from metal carbides with halogen-containing gases such as Cl_2 or HCl.[20] The final products obtained in this way are commonly known as carbide-derived carbons (CDCs). In some carbides the mechanism implies the elimination of the metal from outside to inside of the particle yielding embedded metal carbide nanocrystals in amorphous carbon depending on the temperature treatment.[21] Taking into account these observations and the experience of the group of such kind of reactions, the idea is to apply the chlorination to organometallic precursors that react with chlorine with the same behavior as the carbides described above, yielding and intermediate product composed by nanoparticles of the organometallic precursor embedded on a carbon matrix that could be transformed into the nano-oxide by solvothermal treatments.[22]

Herein, we report a novel and facile procedure to synthesize tetragonal ZrO_2 nanomaterials. The current synthesis (see Figure 1)

Received: February 28, 2011
Published: April 14, 2011

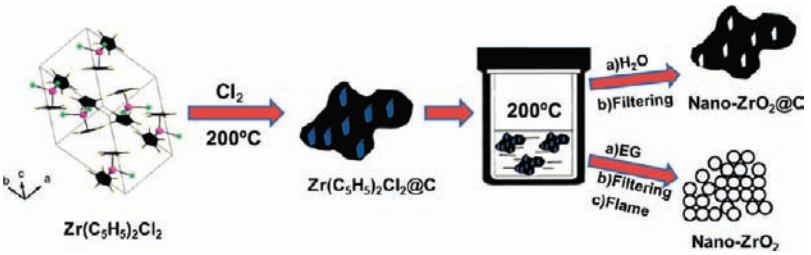

Figure 1. Schematic representation of the synthetic procedure followed in the synthesis of nanometric ZrO_2. On the left a unit cell of the $Zr(C_5H_5)_2Cl_2$ precursor is drawn.

relies upon the chlorination method applied to $Zr(C_5H_5)_2Cl_2$ followed by a solvothermal treatment, where depending on the solvent, ethylene glycol (EG) or water, we produce tetragonal nano-ZrO_2 or embedded ZrO_2 nanocrystals in amorphous carbon (nano-ZrO_2@C).

2. EXPERIMENTAL SECTION

2.1. Synthesis. *(a). Chlorination Reaction.* A 300 mg portion of bis(ciclopentadienyl)zirconium dichloride, ($Zr(C_5H_5)_2Cl_2$), with $P\bar{1}$ space group, (a = 0.8109 nm, b = 1.1845 nm, c = 1.2364 nm, α = 71.08°, β = 76.82°, γ = 87.62°), and melting point 242−245 °C, (Aldrich, powder purity of ≥98%) were placed in a quartz vessel and heated in a tubular furnace at 200, 300, and 600 °C as final temperatures, with a heating rate of 50 °C/min. Continuous flow (25 cm^3/min) of high purity chlorine gas (99.99% Praxair) was inserted while raising the reactor temperature. When the final temperature was reached, the reaction time was set to 30 min. When the reaction time had elapsed, chlorine gas flow was cut and replaced by argon (25 cm^3/min) for removal of the rest of the reacting chlorine and halides during the reactor cooling to room temperature. Chlorine excess and $ZrCl_4$, at the exit of the reactor, were neutralized with a NaOH saturated solution. The possible chlorination reaction that takes place can be described as follows:

$$Zr(C_5H_5)_2Cl_2(s) + 6Cl_2(g) \rightarrow 10C(s) + 10HCl(g) + ZrCl_4(g) \quad (1)$$

(b). Solvothermal Step. A 50 mg portion of the intermediate precursor, $Zr(C_5H_5)_2Cl_2$@C, obtained at 200 °C, was placed in a Teflon stainless steel hydrothermal chamber with 30 mL of the solvent (water or ethylene glycol (EG)). The autoclave was heated at 200 °C for 24 h and depending on the solvent the post-treatments were different. With water as solvent, the sample was filtered under vacuum, and the residual black powder was dried at 100 °C. However, the use of EG yields a black polymer-like residual which was placed in an alumina crucible and calcinated in a flame.

2.2. Characterization. Transmission electron microscopy (TEM) studies were performed in a Philips CM 200FEG electron microscope (point resolution ∼0.23 nm, acceleration voltage of 200 kV), equipped with an EDAX DX-4 detector for X-ray energy dispersive spectroscopy (XEDS) analyses and with a GIF 200 for electron energy-loss spectroscopy (EELS) experiments (energy resolution ∼0.70 eV). High-Resolution and Scanning TEM (STEM) images in high-angle annular dark field (HAADF) mode were obtained with a JEM 3000F microscope (acceleration voltage of 300 kV). TEM specimens were prepared from ultrasonic dispersions of the corresponding samples in butanol. One drop of each suspension was deposited on a copper grid, covered with a holey carbon film. Simulations of the ring patterns were performed with the software MacTempas X,[23] using the structure of the different polymorphs (cubic and tetragonal) of ZrO_2 as input.[24] X-ray powder diffraction patterns (XRPD) were recorded with a Siemens D-501 ($Cu-K_{\alpha 1}$ radiation λ = 0.15406 nm) over the angular range 5−70°, with a step scan of 0.04°.

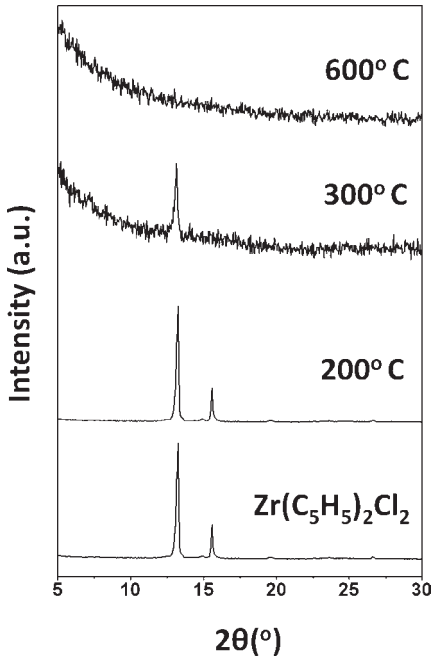

Figure 2. XRPD patterns showing the diffraction maxima of the crystalline starting $Zr(C_5H_5)_2Cl_2$ and the final reaction products. Note that the strongest reflections from the precursor remain until 300 °C. Only at 600 °C is the precursor totally transformed in a disordered carbon material as it is described in reaction 1.

3. RESULTS AND DISCUSSION

3.1. Chlorination Reaction. The evolution of the chlorination reaction of $Zr(C_5H_5)_2Cl_2$ was followed by X-ray powder diffraction data. As it is displayed in Figure 2, the characteristic peaks of $Zr(C_5H_5)_2Cl_2$ detected in the pattern remain until 300 °C. At 600 °C the Bragg reflections of the precursor disappear indicating the complete elimination of the metal yielding a carbonaceous highly disordered material, as it was also confirmed by TEM. For our purpose the most interesting products are those obtained at 200 and 300 °C.

Although, XRPD gives valuable information about the evolution of the precursor under different synthetic conditions, this technique cannot distinguish between a mixture of amorphous carbon and crystalline unreacted precursor and a material

dx.doi.org/10.1021/ic2004112 |Inorg. Chem. 2011, 50, 4640–4646

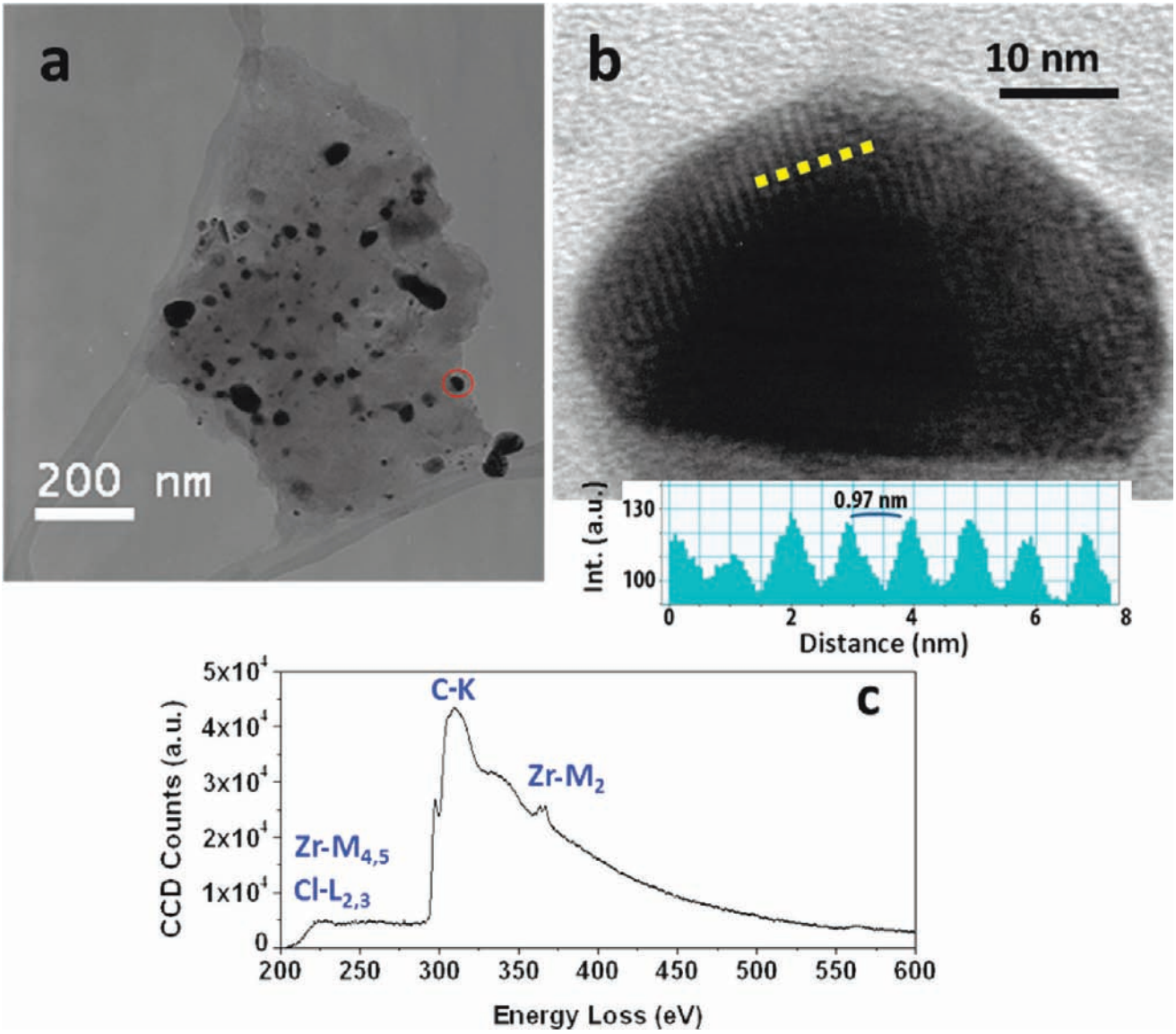

Figure 3. (a) Low magnification TEM image of the $Zr(C_5H_5)_2Cl_2$ chlorinated at 200 °C. (b) HRTEM image of the particle encircled in red in (a). The dotted yellow line represents the line profile displayed below. (c) EEL spectrum recorded in the same particle.

composed by embedded $Zr(C_5H_5)_2Cl_2$ in an amorphous carbonaceous matrix. A TEM study has been performed for this reason. In the low magnification TEM image (Figure 3a), we can clearly observe a typical platelet-like particle of the material obtained at 200 °C. It is composed by dark occluded nanoparticles in a gray amorphous matrix. In the high magnification image of the particle marked by a red circle (Figure 3b), we can detect a row of fringes. The spacing between the fringes, as it has been measured in the line profile across that image, is 0.97 nm, which corresponds to the (110) plane of $Zr(C_5H_5)_2Cl_2$. The chemical elements present in these nanoparticles are determined by EELS and XEDS. The presence of the characteristic edges from Cl, C, and Zr as they are displayed in Figure 3c, which corresponds to the particle marked by a red circle in Figure 3a, confirms that the formation of amorphous carbon protects the precursor from the chlorine attack yielding an interesting intermediate for the preparation of the oxide nanomaterial. In addition, although the Zr-$M_{4,5}$ and Cl-$L_{2,3}$ edges overlap, the presence of Cl is confirmed by XEDS. From these results, although the precursor still remains at 300 °C, the mechanism of the chlorination reaction, where Zr is eliminated as $ZrCl_4$ (bp: 331 °C), suggest that 200 °C is a better choice to synthesize a large amount of nanoparticles.

3.1. Solvothermal Treatment. The transformation of the precursor obtained after chlorination at 200 °C via solvothermal procedures using different solvents was first evaluated by XRPD (see Figure 4). The diffractograms clearly show a complete transformation of the starting material, yielding a pattern characteristic of a disordered material after the treatment with water. However, the alternative procedure using EG followed by calcination yields a pattern where all the maxima can be assigned in the base of the F-centered cubic phase of ZrO_2 *fluorite-type*, but as the tetragonal phase is only a slightly distortion of the cubic one, the presence of broad maxima because of the nanometric nature of the material makes it difficult to distinguish them only using the X-ray data.

dx.doi.org/10.1021/ic2004112 |*Inorg. Chem.* 2011, 50, 4640–4646

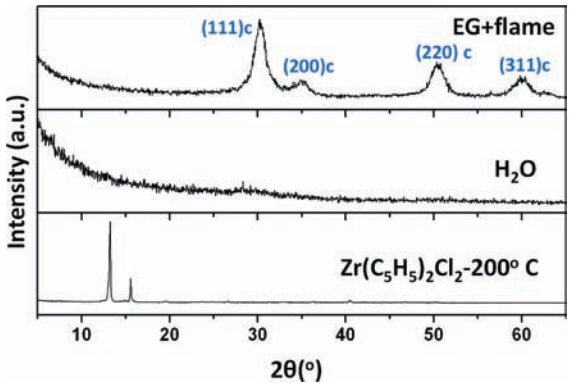

Figure 4. XRPD patterns showing the diffraction maxima of the starting $Zr(C_5H_5)_2Cl_2$@C intermediate synthesized at 200 °C and after the solvothermal treatments.

Under our solvothermal conditions (200 °C), the water and ethylenglycol (EG) are quite different from those at normal conditions because of the autogenous high pressure when the temperature exceeds the boiling points of both solvents. Their different nature yields different products after the treatment; a black powder in the case of water and a polymer with EG, which is transformed to a gray powder after calcination in the flame.

It seems that whereas the water hydrolyzes the $Zr(C_5H_5)_2Cl_2$ and, assisted by the oxygen atmosphere inside the autoclave, promotes the crystallization of nano-ZrO_2 into the carbonaceous matrix, the EG reacts with the intermediate and produce a polymer-like product, where the calcination eliminates the organic material and yields a residual gray powder.

A closer inspection of the sample synthesized in water by High-Resolution transmission electron microscopy (HRTEM) shows interesting details about this sample. Although the XRPD pattern is characteristic of a disordered material, in reality it is a composite material formed by nanocrystalline particles, below 10 nm in diameter, embedded in an amorphous matrix as it can be observed in the HRTEM image displayed in Figure 5a. The EEL spectrum (Figure 5b) from the area marked with a red circle in 5a, gives valuable analytical information, showing the characteristic edges from C, Zr, and O, and therefore suggesting the transformation of nano-$Zr(C_5H_5)_2Cl_2$ into nano-ZrO_2. Besides, the absence of chlorine is confirmed by the absence of signal in the XEDS spectrum.

In the case of composite materials, the calculation of the size distributions from HRTEM images is hazardous and not reliable, because, due to the effect of the thickness and the defocus, we cannot clearly observe the real shape of the nanocrystals, and many of them are invisible because of the defocus effect. In this situation, HAADF images are very helpful, because the intensity of the images is insensitive to the defocus effect and almost proportional to the atomic number Z of the atoms present in the material.[25] In our case the ZrO_2 nanoparticles which contain the heavier zirconium atoms ($Z = 40$) will present a brighter contrast in the HAADF micrograph, as it is shown in Figure 5c where a high amount of nanoparticles embedded in the carbonaceous matrix are clearly observed. From the HAADF image and measuring of 53 particles, the size distribution histogram was obtained, yielding an average diameter of 1.7 ± 0.4 nm for this synthetic procedure (see inset in Figure 5c).

It has been reported that the high-temperature tetragonal phase is stable at room temperature as a consequence of the

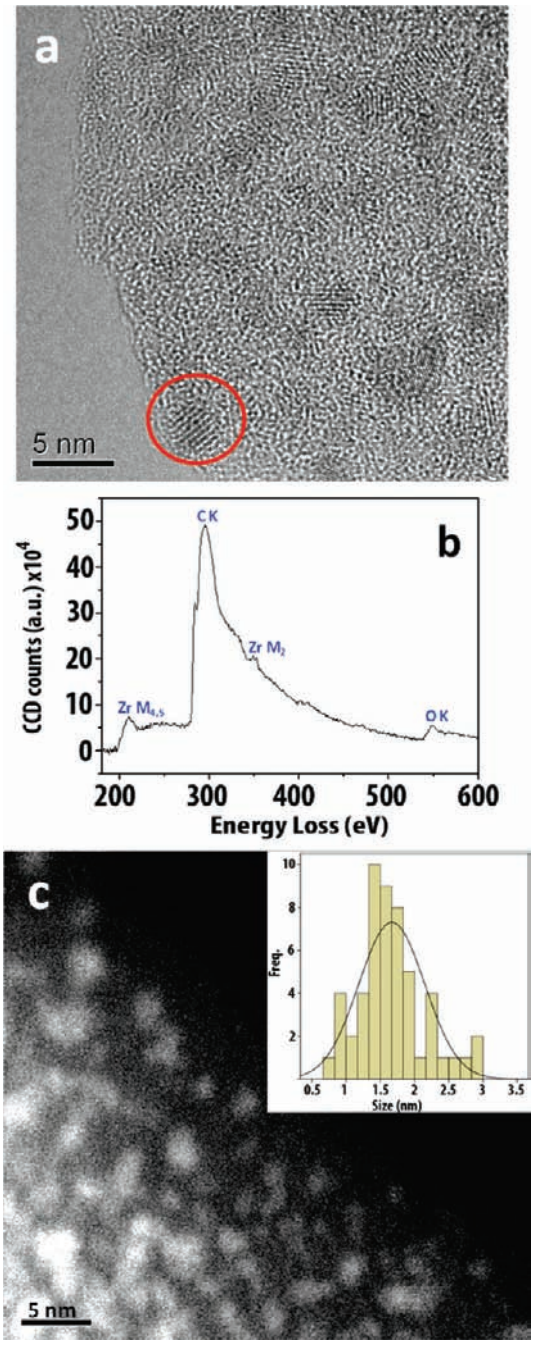

Figure 5. (a) HRTEM micrograph from the composite nano-ZrO_2@C. (b) EEL spectrum taken on the nanoparticle marked with a red circle in (a). (c) HAADF-STEM image. On the upper right corner the size distribution histogram calculated from that image is displayed.

dominance of the surface energy contribution to the Gibbs free energy of formation when the size of the nanoparticles is below 10 nm.[26] Because of the composite nature and nanosize of our material it is not easy to analyze the atomic structure of our ZrO_2 for a clear identification of the polymorph obtained using this methodology. To get further insight into the crystallographic nature of these nanocrystals and their atomic surface, an HRTEM analysis was performed. For this purpose, we need to find oriented nanoparticles on the carbon matrix, where the atomic structure is clearly resolved. In this sense the

dx.doi.org/10.1021/ic2004112 |Inorg. Chem. 2011, 50, 4640–4646

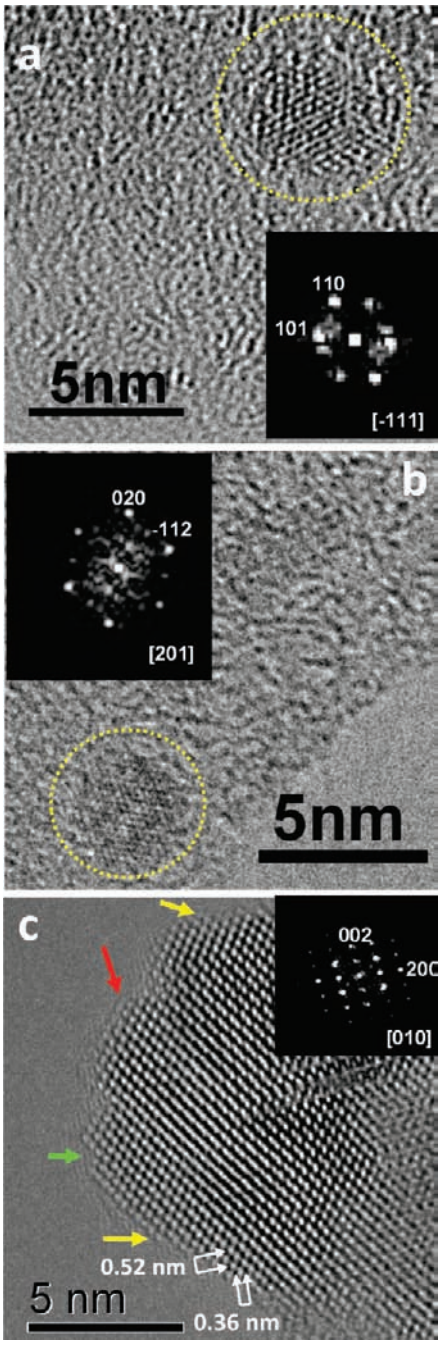

Figure 6. HRTEM images from tetragonal ZrO_2 embedded nanoparticles along (a) [−111], (b) [201], and (c) [010] as it is revealed by the analysis of their digital diffraction patters (DDP) or Fast Fourier Transform (FFT) of the particles encircled in (a) and (b) and the whole particle in (c). Surface defects such as monatomic steps, edges, and surface reconstructions are marked by yellow, red, and green arrows respectively in (c).

nanoparticles imaged in Figure 6 are a good example. The digital diffraction patterns (DDP) or Fast Fourier Transform (FFT) insets in Figure 6 are very helpful and can be interpreted on the base of the tetragonal polymorph of ZrO_2 along the [−111], [201], and [010] zone axes, respectively (see Figures 6a, b, and c). In Figure 6c, we observe the interface between the particle and the carbon matrix, and it shows a variation in contrast due to

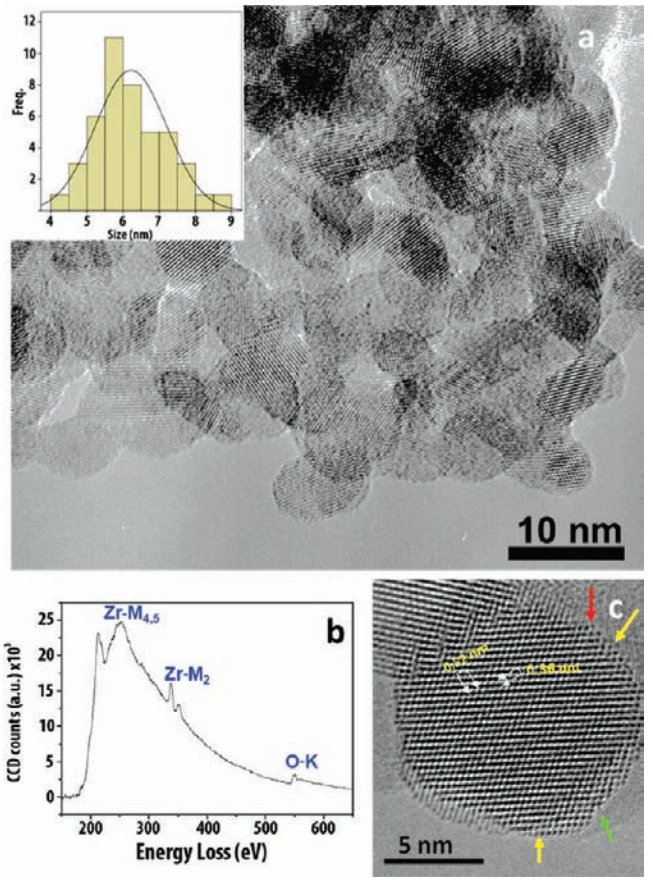

Figure 7. (a) HRTEM micrograph from nano-ZrO_2. This image was used to calculate the size distribution plot inset on the left upper part. (b) EEL spectrum taken in the nanoparticles displayed in (a). (c) HRTEM image from a typical quasi-spherical nanoparticle. The arrows mark different surface defects.

Moiré patterns produced by the overlapping with deeper particles; besides, when we move toward the edge of the particle we note a misorientation and only at the thinner area close to the edge can we clearly observe the atomic structure. This arrangement is characteristic of the projection along the tetragonal [010] zone axis with measured distances of 0.36 and 0.52 nm, which correspond to the *a* and *c* lattice parameters, respectively.

The sample prepared in EG followed by calcination, under the electron microscope is formed by agglomerated crystalline roughly spherical nanoparticles as shown in Figure 7a. Here the size of the nanoparticles can be measured directly (45 particles were used) in the low magnification TEM image (see the histogram inset in Figure 7a), yielding in this case an average diameter of 6.2 ± 0.9 nm. The EEL spectrum confirms again the chemical nature of our material showing only the characteristic edges from Zr and O (see Figure 7b). A HRTEM study has been performed to investigate the atomic structure of these particles. In Figure 7c, one isolated particle is displayed. For a clear comparison, the image was recorded in a particle showing the atomic arrangement along the same zone axis [010] than in the previous material, and therefore both the contrast and the distances between adjacent planes, 0.36 and 0.52 nm, correspond again to the tetragonal phase. This identification is confirmed after the analysis of the ring pattern from the area imaged in Figure 7a. Its interpretation allow us, to determine the crystallographic phase

dx.doi.org/10.1021/ic2004112 |*Inorg. Chem.* 2011, 50, 4640–4646

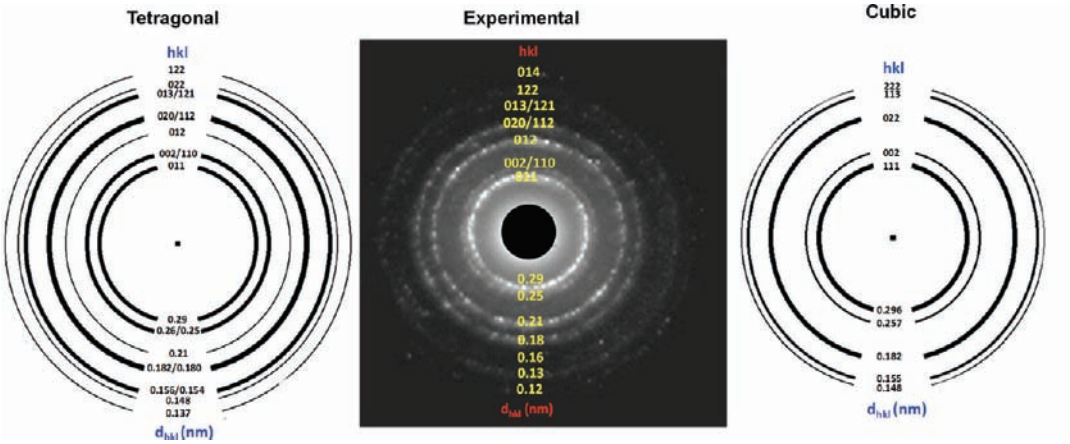

Figure 8. Comparison between the calculated ring patterns from the cubic and tetragonal polymorph of ZrO_2 and the experimental one recorded in the area displayed in Figure 7a.

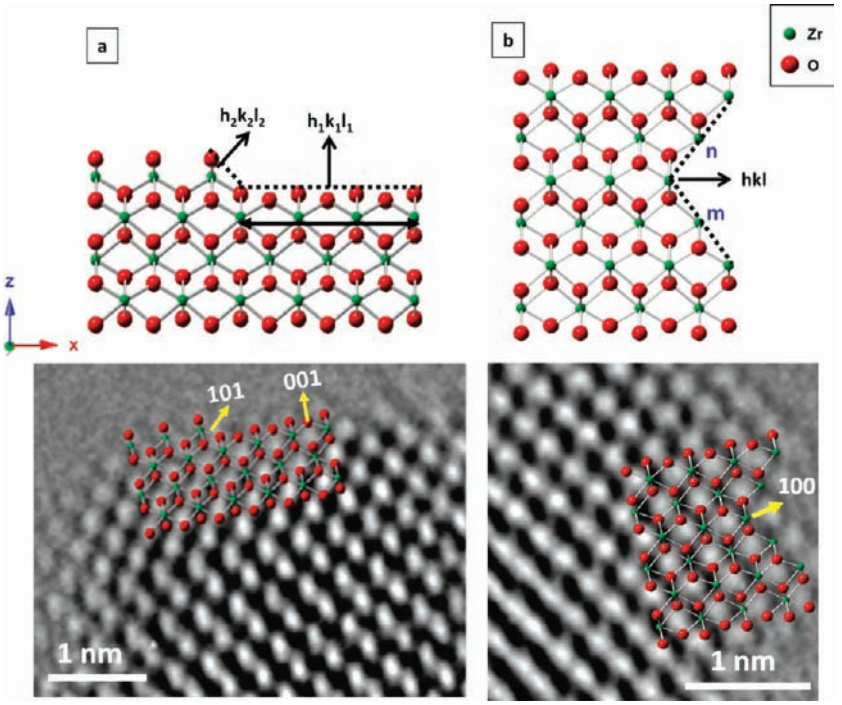

Figure 9. (a) Monoatomic steps using the notation $n(h_1k_1l_1)\times(h_2k_2l_2)$, where the *hkl* indeces describe the terrace and the step planes and *n* the number of atoms on the lower terrace counted from the nanoparticle edge ($n = 4$ in this example). Below an enlargement from the particle imaged in Figure 6c shows this type of step. (b) Surface reconstruction or edges reconstruction. In this case *n* and *m* correspond to the number of atoms on each edge and *hkl* is calculated by the combination of the *hkl* indeces from the edges undergoing the reconstruction. In the example displayed below from the same nanoparticle than in (a), the edges with (101) and (10−1) yield a reconstruction surface (100) with $n = m = 2$, and therefore using the notations it is called (100)-(2 × 2).

if we compare our experimental ring pattern with those simulated for the cubic and tetragonal ZrO_2 polymorphs (see Figure 8). Clearly the experimental pattern fits all the rings calculated for the tetragonal phase, whereas the cubic ZrO_2 exhibits less diffraction rings.

Since the surface atoms in nanocrystals have less bonds in comparison to those in the bulk because of the loss in nearest neighbors, they are likely to have dangling bonds and tend to find new equilibrium positions to balance the forces, resulting in surface defects[27] (steps and reconstructions) and higher surface reactivity. In this sense, since HRTEM has the ability to probe the positions of atomic columns, it is a powerful technique to directly interpret surface defects. In both images, Figure 6c and 7c, taken at the Scherzer[28] defocus, the surface steps and edges are clearly visible and marked with colored arrows. Several features regarding surface defects are noteworthy and for a clear understanding they are represented in Figure 9. The main defects observed in the nanoparticles consist of monatomic steps of the type $n(001)\times(101)$ and $n(101)\times(001)$ (yellow arrows), where the notation $n(h_1k_1l_1)\times(h_2k_2l_2)$, describe the *hkl* indices of the

dx.doi.org/10.1021/ic2004112 |*Inorg. Chem.* 2011, 50, 4640–4646

terrace and the step planes and *n* the number of atoms on the lower terrace counted from the nanoparticle edge. In Figure 9a, a monatomic step of the type 4(001)×(101) is schematically drawn on top, using the projected structure of ZrO_2, and overlapped over the area marked with the yellow arrow in the upper part of Figure 6c. The other kind of surface defects consists on the concurrence of two type of edges (001)/(101) and (101)/(10−1), very sharp in the first situation (red arrows) and they have reconstructed into a (100)-(2 × 2) structure in the latter (green arrows). The second situation is represented in Figure 9b. The values of *n* and *m* correspond to the number of atoms on each edge and *hkl* is calculated by the combination of the *hkl* indeces from the concurrent edges undergoing the reconstruction. In the example the edges (101) and (101) from the particle of Figure 6c yield a reconstruction surface (100) with *n* = *m*= 2, and therefore using the notations is called (100)-(2 × 2).

We should note that although those situations are presented in both materials, they are more pronounced in the embedded nanoparticle, maybe because the treatment under the flame of the material polymerized with EG allows to organize the surface.

4. CONCLUSIONS

To the best of our knowledge, we have applied a synthetic strategy for the first time to produce oxide nanomaterials based on the combination of the chlorination and solvothermal reactions. This strategy takes advantage that the chlorination of $Zr(C_5H_5)_2Cl_2$ produces at temperatures below its melting point an intermediate composed by nanoparticles of the precursor embedded in an amorphous carbonaceous matrix. The solvothermal treatment of this intermediate yields tetragonal ZrO_2 nanoparticles (with average size below 10 nm), but depending on the chemical pathway (use of EG + calcination or water + filtering) the nanoparticles are free or embedded in amorphous carbon forming a composite material. For this study, the use of precise electron microscopy techniques such as HRTEM, HAADF, and EELS, allows to determine the chemical composition and structure of the nanoparticles, to measure their size, and to analyze the surface defects at the atomic level.

AUTHOR INFORMATION

Corresponding Author

*Phone: +34-91394-5161. Fax: +34-91394-4352. E-mail: avilad@quim.ucm.es.

ACKNOWLEDGMENT

This work was supported by the projects with references S-2009/PPQ-1626 and MAT2010-19460.

REFERENCES

(1) *Nanoparticles: Building Blocks for Nanotechnology*; Rotello, V., Ed.; Springer: New York, 2004.
(2) He, D.; Ding, Y.; Luo, H.; Li, C. *J. Mol. Catal.* **2004**, *208*, 267–271.
(3) Wilk, G. D.; Wallace, R. M.; Anthony, J. M. *J. Appl. Phys.* **2001**, *89*, 5243–5275.
(4) Wang, G.; Meng, F.; Ding, C.; Chu, P. K.; Liu, X. *Acta Biomater.* **2010**, *6*, 990–1000.
(5) León, C.; Lucia, M. L.; Santamaría, J. *Phys. Rev. B* **1997**, *55*, 882–887.
(6) Shin, J. H.; Chao, C. C.; Huang, H.; Prinz, F. B. *Chem. Mater.* **2007**, *19*, 3850–3854.
(7) Garvie, R. C.; Hannink, R. H.; Pascoe, R. T. *Nature* **1975**, *258*, 703–704.
(8) Garvie, R. C. *J. Phys. Chem.* **1978**, *82*, 218–224.
(9) Shukla, S.; Seal, S.; Vij, R.; Bandyopadhyay, S.; Rahman, Z. *Nano Lett.* **2002**, *2*, 989–993.
(10) Somiya, S.; Akiba, T. *J. Eur. Ceram. Soc.* **1999**, *19*, 81–87.
(11) Li, L. R.; Wang, W. Z. *Solid State Commun.* **2003**, *127*, 639–643.
(12) Woudenberg, F. C. M.; Sager, W. F. C.; Sibelt, N. G. M.; Verweij, H. *Adv. Mater.* **2001**, *13*, 514–516.
(13) Liang, J.; Deng, Z.; Jiang, X.; Li, F.; Li, Y. *Inorg. Chem.* **2002**, *41*, 3602–3604.
(14) Joo, J.; Yu, T.; Kim, Y. W.; Park, H. M.; Wu, F.; Zhang, J. Z.; Hyeon, T. *J. Am. Chem. Soc.* **2003**, *125*, 6553–6557.
(15) Garnweitner, G.; Goldenberg, L. M.; Sakhno, O. V.; Antonietti, M.; Niederberger, M.; Stumpe, J. *Small* **2007**, *3*, 1626–1632.
(16) Clavel, G.; Willinger, M. G.; Zitoun, D.; Pinna, N. *Eur. J. Inorg. Chem.* **2008**, 863–868.
(17) Pucci, A.; Clavel, G.; Willinger, M. G.; Zitoun, D.; Pinna, N. *J. Phys. Chem. C* **2009**, *113*, 12048–12058.
(18) Laidani, N.; Micheli, V.; Anderle, M. *Thin Solid Films* **2001**, *382*, 23–29.
(19) Randeniya, L.; Bendavid, A.; Martin, P.; Cairney, J.; Sullivan, A.; Webster, S.; Proust, G.; Tang, F. Z.; Rohanizadeh, R. *Acta Biomater.* **2010**, *6*, 4154–4160.
(20) Gogotsi,Y. *Nanomaterials handbook*; CRC Press: Boca Raton, FL, 2006.
(21) González-García, P.; Urones-Garrote, E.; Ávila-Brande, D.; Gómez-Herrero, A.; Otero-Díaz, L. C. *Carbon* **2010**, *48*, 3667–3675.
(22) Lojkowski, W.; Gedanken, A.; Grzanka, E.; Opalinska, A.; Strachowski, T.; Pielaszek, R.; Tomaszewska-Grzeda, A.; Yatsunenko, S.; Godlewski, M.; Matysiak, H.; Kurzydłowski, K. J. *J. Nanopart. Res.* **2008**, *11*, 1991–2002.
(23) *MacTempas X*; A program for simulating HRTEM images and diffraction patterns, Version 2.3.7; Total Resolution: Berkeley, 2010.
(24) Howard, C. J.; Hill, R. J.; Reichert, B. E. *Acta Crystallogr.* **1988**, *B44*, 116–120.
(25) Nellist, P. D. *Scanning transmission electron microscopy*; Hawkes, P. W., Spence, J. C. H., Eds.; Springer: New York, 2007; Science of Microscopy, Vol. 1.
(26) Garvie, R. C.; Goss, M. F. *J. Mater. Sci.* **1986**, *21*, 1253–1257.
(27) Zhu, X.; Wang, J.; Zhang, Z.; Zhu, J.; Zhou, S.; Liu, Z.; Ming, N. *J. Am. Ceram. Soc.* **2008**, *91*, 1002–1008.
(28) Williams, D. B.; Carter, C. B. *Transmission Electron Microscopy: A Textbook for Materials Science*; Springer: New York, 2009.